Tadeusz NIEDZIELA

Warsaw University of Technology, Faculty of Transport

(Hg,Zn)Te Photon Detectors of Thermal Radiation

Streszczenie. *Określono rozkład fali elektromagnetycznej w typowej strukturze detekcyjnej detektora fotonowego. Podano wzory na: współczynnik zewnętrznej wydajności kwantowej oraz rozkład intensywności promieniowania w elemencie fotoczułym. Obliczono maksymalne do uzyskania parametry detekcyjne fotorezystorów z (Hg,Zn)Te. Zilustrowano współczynnik zewnętrznej wydajności kwantowej oraz intensywność promieniowania w elemencie fotoczułym umieszczonym w optymalnej optycznej wnęce rezonansowej. Obliczono graniczne znormalizowane wykrywalności termiczne niechłodzonych (T=300K) detektorów fotonowych z (Hg,Zn)Te.* ***Fotonowe detektory promieniowania termicznego (Hg,Zn)Te***

Abstract*. Distribution of electromagnetic wave has been determined in a typical detection structure of a photon detector. Formulas have been given for: external quantum efficiency and distribution of radiation intensity in a photosensitive element. Maximal detection parameters of (Hg,Zn)Te photoresistors have been calculated. External quantum efficiency and radiation intensity in a photosensitive element located in the optimal optical resonance cavity have been illustrated. Ultimate normalized thermal detectivity of the uncooled (T=300K) (Hg,Zn)Te photon detectors has been calculated.*

Słowa kluczowe: detektory fotonowe, intensywność promieniowania, współczynnik zewnętrznej wydajności kwantowej, wykrywalność termiczna.
Keywords: photon detectors, radiation intensity, external quantum efficiency, thermal detectivity

doi:10.12915/pe.2014.07.09

Introduction

Currently, for the purpose of positioning the motor vehicles on the road and transport management within the intelligent transport systems, sensors operating on the basis of various physical phenomena or operating within various ranges of electromagnetic radiation spectra are widely used. It has become standard practice to apply the thermographic cameras on motorways, which allow for identification of objects in difficult atmospheric conditions. Designing efficient image sensors requires research and optimization of detection parameters of single elements as well as whole matrices of electromagnetic sensors.

Fast development of thermal imaging devices is mainly connected with the development of infrared detector technology forced by space, military and industrial needs. IR detectors have been used in common use appliances, in monitoring and access and steering systems. For many years, intensive researches have been conducted on IR photodetectors on the basis of narrow-bandgap semiconductors, which make use of the phenomenon of optical generation of electron-hole pairs [1-13].

The main material applied in the construction of photon detectors are narrow-bandgap semiconductors on the basis of mercury telluride ((Hg,Cd)Te, (Hg,Mn)Te and (Hg,Zn)Te). The most commonly used material, however, is mercury cadmium telluride due to its unique properties which allow for construction of detectors in a wide range of long-wavelength edge of photosensitivity [6]. This material, however, is difficult to obtain in industrial production from technological point of view. Instability of crystal network and surface of this type of semiconductor, as well as lack of durability of interface make it necessary to serach for the new semiconductors. Therefore, attempts have been made to substitute this semiconductor by others.

A promising narrow-bandgap semiconductor is (Hg,Zn)Te [7-13] due to the fact that crystals (Hg,Zn)Te characterize of lower density of macroscopic defects in comparison with commonly used crystals (Hg,Cd)Te. This semiconductor is more resistant to plastic deformation and dislocations than (Hg,Cd)Te, whereas their component dependencies of transport and optical properties are similar.

The medium wavelength infrared detectors (MWIR) require light cooling (thermoelectric cooling (T=200K)) in order to obtain BLIP conditions, whereas the long wavelength infrared detectors (LWIR) require a deep cooling (cryogenic cooling (≅77 K)). The necessity of a deep cooling, significantly increases the cost, size, weight, power consumption and inconvenience of construction. Uncooled detectors are in turn of small sizes, they are light and convenient in use.

The increased interest in the high-temperature (300–200K) infrared photon detectors of a medium wavelength (3–5.5μm) and long wavelength (8-14μm) is connected with development of photodiodes, photoresistors, photoelectromagnetic detectors and Dember detectors for areas of high electromagnetic radiation transmission. There is a high demand for homogeneous detectors of a big area for research purposes, as well as of a small area as the single mosaic elements. Within a wide range, their sensitivity, size and power consumption changes.

The main objective in the construction of photon detectors is obtaining the BLIP conditions (in which the noise is lowered to the background level) at the highest possible operating temperature. The ultimate goal is to obtain a near - BLIP detectivity at room temperature or at least a at higher temperatures (e.g. obtained as a result of thermoelectric cooling). The increasing detection parameters of the photon detectors are realized by means of optimization of construction and material parameters of the optical resonance cavity, the optical immersion and the attenuation of generation and recombination processes.

Formulating a detection problem

It is best to analyze a distribution of the electric ($\vec{E}$) and magnetic ($\vec{B}$) fields in detection structure using Maxwell's equations.

Maxwell's equation for linear isotropic center takes the form [14].

$$\nabla \cdot \vec{B} = 0$$

$$\nabla \cdot \vec{E} = 4\pi\rho$$

$$\nabla \times \left(\frac{\vec{B}}{4} \right) = \frac{1}{c} \cdot \frac{\partial \left(\varepsilon \vec{E} \right)}{\partial t} + \frac{4\pi}{c} \vec{j}$$

$$\nabla \times \vec{E} = -\frac{1}{c} \cdot \frac{\partial \vec{B}}{\partial t}$$

Let us assume for the sake of simplification that in the analyzed centers, the density of charges and currents ($\rho = 0$, $\vec{j} = 0$) equal zero and the values of magnetic permeability μ are identical.

Therefore, Maxwell's equations take the following form:

(1) $\nabla \cdot \vec{B} = 0$

(2) $\nabla \cdot \vec{\mathrm{E}} = 0$

(3) $\nabla x\left(\frac{\vec{\mathrm{B}}}{4}\right) = \frac{1}{c} \cdot \frac{\partial\left(\varepsilon \vec{\mathrm{E}}\right)}{\partial t}$

(4) $\nabla x \vec{\mathrm{E}} = -\frac{1}{c} \cdot \frac{\partial \vec{\mathrm{B}}}{\partial t}$

Conducting operations of rotation on equations (3) and (4) and making use of relations (1) ÷(4) and vector identities we obtain:

$$\nabla^2 \vec{\mathrm{B}} - \frac{\mu\varepsilon}{c^2} \frac{\partial^2 \vec{\mathrm{B}}}{\partial t^2} = 0,$$

$$\nabla^2 \vec{\mathrm{E}} - \frac{\mu\varepsilon}{c^2} \frac{\partial^2 \vec{\mathrm{E}}}{\partial t^2} = 0$$

Both $\vec{\mathrm{B}}$ and $\vec{\mathrm{E}}$ fulfill identical wave equation, that is each component B_i, E_i fulfills the equation:

$$\nabla^2 \Psi(x,y,z,t) - \frac{\mu\varepsilon}{c^2} \frac{\partial^2 \psi(x,y,z,t)}{\partial t^2} = 0$$

Let the function ψ be expressed in the form:

$$\Psi(x,y,z,t) = \varphi(x,y,z) e^{i\omega t}$$

we obtain

(5) $\nabla^2 \varphi(x,y,z) + k^2 \varphi(x,y,z) = 0$

$$k^2 = \mu\varepsilon \frac{\omega^2}{c^2}$$

where $\vec{k}$ is the phase vector.

In accordance with a classic definition of refraction coefficient

$$n^2 = \mu\varepsilon$$

we have:

$$k^2 = \mu\varepsilon \frac{\omega^2}{c^2} = n^2 \frac{\omega^2}{c^2}$$

The solution of the equation (5) is the function

$$\varphi(x,y,z) = exp\left[\pm i\left(k_x x + k_y y + k_z z\right)\right]$$

where

$$k_x^2 + k_y^2 + k_z^2 \equiv k^2 = n^2 \frac{\omega^2}{c^2} = \mu\varepsilon \frac{\omega^2}{c^2}$$

Generally we then have:

$$\psi(x,y,z,t) = e^{i(\pm \vec{k}\vec{r} + \omega t)} .$$

Let

$$k_z \neq 0,\ k_x = k_y = 0$$

then the general solution contains one plane wave in the direction of +z and one in the direction of -z:

$$\psi(z,t) = \left[A^+ e^{izk} + A^- e^{-izk}\right] e^{i\omega t}$$

The assumed directions ±k are symbolic. The considerations will be conducted for +k as propagation in the direction of +z, whereas, −k for the direction of −z. After introducing the ultimate formula, we will change ± k into opposite signs k (it does not change the rule of generality).

As the propagation is in the direction of ±z, therefore,

$$\nabla \cdot \vec{B} = 0 \rightarrow \mathrm{B_z} = \mathrm{const}$$

$$\nabla \cdot \vec{E} = 0 \rightarrow \mathrm{E_z} = \mathrm{const}$$

Constancy of $\mathrm{B_z}$, $\mathrm{E_z}$ is only possible for frequency $\omega = 0$. This case as not being physical, will not be considered, that is, $\mathrm{B_z} = 0,\ \mathrm{E_z} = 0$. What remains, generally speaking, is two components of electric field $\mathrm{E_x}$, $\mathrm{E_y}$ and two components of induction field $\mathrm{B_x}$, $\mathrm{B_y}$. For the sake of simplification we assume linear polarization with the values $\mathrm{E_x} \neq 0,\ \mathrm{E_y} = 0$, which generally means:

(6) $\mathrm{E_x}(z,t) \equiv E = \left(\mathrm{A^+ e^{ikz}} + \mathrm{A^- e^{-ikz}}\right) \mathrm{e^{i\omega t}}$

$E_y = E_z = 0$

Therefore, from Maxwell's equations (3) and (4) we obtain:

$$\frac{\partial B_y(z,t)}{\partial z} = -\frac{\mu\varepsilon}{c} \frac{\partial E_x}{\partial t} \quad ,$$

$$\frac{\partial B_y}{\partial t} = -c \frac{\partial E_x}{\partial z}$$

where it can be easily seen that the magnetic induction

(7) $B_y(z,t) \equiv B = n\left(A^+ e^{ikz} - A^{-ikz}\right) e^{i\omega t}$

$B_x = B_z = 0$

Obtained dependencies (6), (7) are interesting for us from the point of view of technical applications and constitute a general form of solutions of Maxwell's equations for the problem of thermal radiation detection.

Boundary conditions

On the border of the centers we have physical discontinuity. On both sides of the border, the equations (1)÷(4) are fulfilled, but the fact should be taken into consideration that these centers are different.

Having a general form of solutions (6) and (7) for vectors $\vec{E}$ *and* $\vec{B}$ we will write:

(8) $\nabla x\left(\frac{\vec{\mathrm{B}}}{\mu}\right) = \frac{1}{c} \frac{\partial\left(\varepsilon \vec{\mathrm{E}}\right)}{\partial t} \equiv i \frac{\omega}{c} \varepsilon \vec{\mathrm{E}}$

$$\nabla x \vec{\mathrm{E}} = -\frac{1}{c} \frac{\partial \vec{\mathrm{B}}}{\partial t} = -i \frac{\omega}{c} \vec{\mathrm{B}}$$

It should be noticed that in our case $\vec{E} = \vec{x}E_x$, $B = \vec{y}B_y$ ($\vec{x}$, $\vec{y}$ – *unit vectors*).

The Stokes equation is binding for any vector $\vec{F}$

$$(9) \qquad \int \left(\nabla \times \vec{F}\right) d\vec{A} = \oint \vec{F} \cdot d\vec{l}$$

where: $d\vec{A}$ – *surface element*, $d\vec{l}$ is the linear element along the curve including this surface.

We shall use the Stokes equation for the vectors $\vec{E}$ *and* $\frac{\vec{B}}{\mu}$ choosing integration on the border of two centers.

Applying $\lim \Delta z \to 0$ we get, $\int \left(\nabla \times \vec{F}\right) \cdot d\vec{A} \to 0$, because they are the physical fields and their rotations are limited. It leads to the following dependency:

$$(10) \quad \oint \vec{F} \cdot d\vec{l} = 0 \quad \rightarrow \quad \vec{F_2}\Delta l - \vec{F_1}\Delta l = 0$$

Finally we have tangent components E and B/μ which are continuous on the border of centers.

Distribution of electric field in detection structure

Making use of the introduced general solutions in the form of (6) and (7), a model of electric field distribution can be proposed in the layer detection structure (Fig. 1).

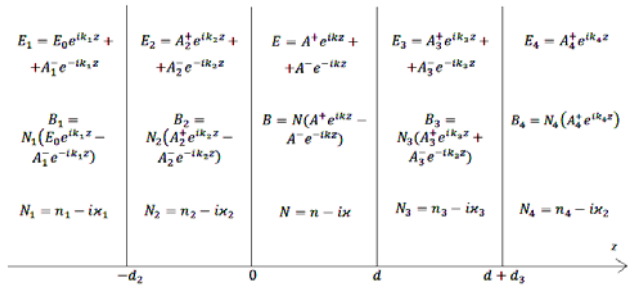

Fig. 1. Electric field distribution scheme in layer detection structure

For determining of the eight constants of Fig. 1 $\left(A_1^-, A_2^+, A_2^-, A^+, A^-, A_3^+, A_3^-, A_4^-\right)$, the eight boundary conditions should be established:

$$(11) \quad E_1|_{z=-d_2} = E_2|_{z=-d_2}, \qquad \left.\frac{B_1}{\mu}\right|_{z=-d_2} = \left.\frac{B_2}{\mu}\right|_{z=-d_2}$$

$$E_z|_{z=0} = E|_{z=0}, \qquad \left.\frac{B_2}{\mu}\right|_{z=0} = \left.\frac{B}{\mu}\right|_{z=0}$$

$$E|_{z=d} = E_3|_{z=d}, \qquad \left.\frac{B}{\mu}\right|_{z=d} = \left.\frac{B_3}{\mu}\right|_{z=d}$$

$$E_3|_{z=d+d_3} = E_4|_{z=d+d_3}, \qquad \left.\frac{B_3}{\mu}\right|_{z=d+d_3} = \left.\frac{B_4}{\mu}\right|_{z=d+d_3}$$

Substituting functions E_i, B_i given in Fig.1, in the above boundary conditions we obtain the field distribution E in the photosensitive element (0<z<d)

$$(12) \quad E = E_0 T_1 T_2 i^{i\omega t} e^{-i(k_1 - k_2)d_2} \cdot \frac{\left(e^{-ik_3 2d_3} - r_3 r_4\right)e^{-ik(2d-z)} - \left(r_4 - r_3 e^{-ik_3 2d_3}\right)e^{-ikz}}{\left(r_2 + r_1 e^{ik_2 2d_2}\right)\left(r_4 - r_3 e^{-ik_3 2d_3}\right) + \left(1 + r_1 r_2 e^{-k_2 2d_2}\right)\left(e^{-ik_3 2d_3} - r_3 r_4\right)e^{ik2d}}$$

Now we change $\pm k_i$ *into* $\mp k_i$.

After simple conversions we obtain a dependency for the electric field distribution in a photosensitive layer 0<z<d.

$$(13) \quad E_0 = E_0 T_1 T_2 e^{i\omega t} e^{i(k_1 - k_2)d_2} \cdot \frac{\left(e^{ik_3 2d_3} - r_3 r_4\right)e^{-ikz} + \left(r_3 e^{-ik_3 2d_3} - r_4\right)e^{-ik(2d-z)}}{\left(1 + r_1 r_2 e^{-ik_2 2d_2}\right)\left(e^{-ik_3 2d_3} - r_3 r_4\right) - \left(r_2 + r_1 e^{-ik_2 2d_2}\right)\left(r_3 e^{-ik_3 2d_3} - r_4\right)e^{-ik2d}}$$

where:

$$(14) \quad \omega = \frac{2\pi}{\lambda}c,$$

$$k = \frac{2\pi}{\lambda}N, \quad k_1 = \frac{2\pi}{\lambda}N_1, \quad k_2 = \frac{2\pi}{\lambda}N_2, \quad k_3 = \frac{2\pi}{\lambda}N_3$$

$$T_1 = \frac{2N_1}{N_1 + N_2}, \quad T_2 = \frac{2N_2}{N + N_2}$$

$$r_1 = \frac{N_2 - N_1}{N_2 + N_1}, \quad r_2 = \frac{N - N_2}{N + N_2}, \quad r_3 = \frac{N - N_3}{N + N_3}, \quad r_4 = \frac{N_4 - N_3}{N_4 + N_3}$$

For the specific case (photosensitive layer located in two semi-infinite centers)

$$N = n, \quad N_1 = N_2 = n_1, \quad N_3 = N_4 = n_2$$

$$d_2 = d_3 = 0$$

$$k_1 = k_2$$

$$r_1 = r_4 = 0, \quad r_2 = \frac{n - n_1}{n + n_2} \equiv R_1, \quad r_3 = \frac{n - n_2}{n + n_2} \equiv R_2$$

$$T_1 = 1, \quad T_2 = \frac{2n_1}{n + n_1} \equiv T$$

we obtain

$$E = E_0 T e^{i\frac{2\pi}{\lambda}ct} \cdot \frac{e^{-ikz} + R_2 e^{-ik(2d-z)}}{1 - R_1 R_2 e^{-ik2d}}.$$

Let us introduce the following notations:

$$k_0 = \frac{2\pi}{\lambda}N = \frac{2\pi}{\lambda}(n - i\chi) = \frac{\gamma}{2} - i\frac{\alpha}{2}$$

$$\frac{2\pi}{\lambda}\chi = \frac{\alpha}{2}$$

$$\alpha = \frac{4\pi\chi}{\lambda}$$

Thus, we obtain

$$E = TE_0 e^{i\frac{2\pi}{\lambda}ct} \cdot \frac{exp\left(-\frac{\alpha + i\gamma}{2}z\right) + R_2 exp\left(-\frac{\alpha + i\gamma}{2}(2d - z)\right)}{(1 - R_1 R_2)exp(-k\omega) - \left(exp(-i\gamma\omega)\right)}$$

Radiation intensity distribution in a photosensitive element

Radiation intensity distribution in a photosensitive element we shall define as:

$$(13) \quad I = \frac{\lambda}{hc}\sqrt{\frac{\varepsilon}{\mu}}EE^* \text{ we determine } I \approx EE^* \text{ using}$$

$$I = \frac{\lambda}{hc}\frac{P}{lw}EE^*$$

therefore,

$$(14)\quad I = I_0\left\{e^{-sz}A + e^{sz-2K}B + 2e^{-K}\left[\begin{array}{l}\left(\begin{array}{l}R_3R_4[R_4\sin(tz+\varphi_3-\Gamma)-\\ -R_3e^{K_3}\sin(tz+\varphi_4-\Gamma+\Gamma_3)]\end{array}\right)+\\ +\left(\begin{array}{l}+e^{K_3}[-R_3e^{K_3}\sin(tz-\varphi_3-\Gamma)+\\ +R_4\sin(tz-\varphi_4-\Gamma-\Gamma_3)]\end{array}\right)\end{array}\right]\right\}$$

where:

$$(15)\quad I_0 = \frac{\lambda}{hc}\frac{P}{lw}\cdot\left[(1-g_1)^2+h_1^2\right]\left[(1-g_2)^2+h_2^2\right]\cdot$$
$$\cdot\left\{\left|\begin{array}{l}\left(1+r_1r_2e^{-(K_2+i\Gamma_2)}\right)\left(e^{K_3+i\Gamma_3}-r_3r_4\right)-\\ -\left(r_2+r_4e^{-(K_2+i\Gamma_2)}\right)\cdot\left(r_3e^{K_3+i\Gamma_3}-r_4\right)e^{-(K+i\Gamma)}\end{array}\right|^2\right\}^{-1}$$

$$\alpha = s = \frac{4\pi\chi}{\lambda},\quad K = sd,\ \Gamma = td,\quad t = \frac{4\pi n}{\lambda}$$
$$K_2 = \frac{4\pi\chi_2}{\lambda}d_2,\quad \Gamma_2 = \frac{4\pi n_2}{\lambda}d_2,\quad K_3 = \frac{4\pi\chi_3}{\lambda}d_3,$$
$$\Gamma_3 = \frac{4\pi n_3}{\lambda}d_3,\quad R_3 = |r_3|,\quad R_4 \neq |r_4|$$
$$A = e^{2K_3} + R_3^2R_4^2 + 2R_3R_4e^{K_3}\cos(\varphi_3+\varphi_4+\Gamma_3)$$
$$B = R_3^2e^{2K_3t} + R_4^2 - 2R_3R_4e^{K_3}\cos(\varphi_3-\varphi_4-\Gamma_3)$$

$$g_1 = \frac{n_2^2-n_1^2+\chi_2^2-\chi_1^2}{(n_2+n_1)^2+(\chi_2+\chi_1)^2},\quad h_1 = \frac{2(n_2\chi_1-n_1\chi_2)}{(n_2+n_1)^2+(\chi_2+\chi_1)^2}$$
$$g_2 = \frac{n^2-n_2^2+\chi^2-\chi_2^2}{(n+n_2)^2+(\chi+\chi_2)^2},\quad h_2 = \frac{2(n\chi_2-n_2\chi)}{(n+n_2)^2+(\chi+\chi_2)^2}$$
$$g_3 = \frac{n^2-n_3^2+\chi^2-\chi_3^2}{(n+n_3)^2+(\chi+\chi_3)^2},\quad h_3 = \frac{2(n\chi_3-n_3\chi)}{(n+n_3)^2+(\chi+\chi_3)^2}$$
$$g_4 = \frac{n_4^2-n_3^2-\chi_3^2+\chi_4^2}{(n_4+n_3)^2+(\chi_4+\chi_3)^2},\quad h_4 = \frac{2(n_4\chi_3-n_3\chi_4)}{(n_4+n_3)^2+(\chi_4+\chi_3)^2}$$

$$\sin\varphi_3 = \frac{g_3}{R_3},\quad \cos\varphi_3 = \frac{h_3}{R_3}$$
$$\sin\varphi_4 = \frac{g_4}{R_4},\quad \cos\varphi_4 = \frac{h_4}{R_4}$$

For the case of a layer of thickness d surrounded by two semi-infinite non-absorbing dielectrics we obtain:

$$I = I_0\left[e^{-\alpha z} + |R_2|^2e^{\alpha z-2\alpha d} + 2|R_2|e^{-\alpha d}\sin(\gamma z+\varphi-\Gamma)\right]$$
$$I_0 = \frac{\lambda}{hc}\frac{P}{lw}\left\{\begin{array}{l}1+\left(g_1^2+h_1^2\right)\left(g_2^2+h_2^2\right)e^{-2\alpha d}+\\ +2e^{-2\alpha d}\left[(g_1g_2-h_1h_2)\cos\Gamma+(g_1h_2+h_1g_2)\sin\Gamma\right]\end{array}\right\}^{-1}$$
$$|R_2| = \sqrt{g_2^2+h_2^2}$$
$$R_3 = R_2$$

The external quantum efficiency η can be defined as:

$$\eta = \int_0^d I(z)dz$$

thus, we obtain

$$\eta = I_0\left[A+(B-A)e^{-K}-Be^{-2K}\right] - \frac{4I_0}{t}\sin\frac{\Gamma}{2}e^{-K}\cdot$$
$$\cdot\left\{\begin{array}{l}R_3R_4\left[e^{K_3}R_3\sin\left(\varphi_4+\Gamma_3-\frac{\Gamma}{2}\right)-R_4\sin\left(\varphi_3-\frac{\Gamma}{2}\right)\right]+\\ +e^{K_3}\left[R_4\sin\left(\varphi_4+\Gamma_3+\frac{\Gamma}{2}\right)-R_3e^{K_3}\sin\left(\varphi_3+\frac{\Gamma}{2}\right)\right]\end{array}\right\}$$

The amplitude reflectance $\left(R\equiv\frac{A_1^-}{E_0}\right)$ and transmission $\left(\mathrm{T}\equiv\frac{A_4^+}{E_0}\right)$ coefficients for such a multi-layer scheme assumed (Fig. 1) equal:

$$R \equiv A_1^- = E_0e^{ik_id_2}\cdot\frac{C-D}{E}$$
$$C = \left(r_1+r_2e^{-ik_2 2d_2}\right)\left(e^{ik_3 2d_3}-r_3r_4\right)$$
$$D = \left(r_1r_2+e^{-ik_2 2d_2}\right)\left(r_3e^{ik_3 2d_3}-r_4\right)e^{-ik2d}$$
$$E = \left(1+r_1r_2e^{-ik_2 2d_2}\right)\left(e^{ik_3 2d_3}-r_3r_4\right)-$$
$$-\left(r_2+r_1e^{-ik_2 2d_2}\right)\left(r_3e^{ik_3 2d_3}-r_4\right)e^{-ik2d}$$
$$\mathrm{T} \equiv A_4^+ = \mathrm{T}_1\mathrm{T}_2\mathrm{T}_3\mathrm{T}_4\cdot\frac{e^{ik_1d_2}e^{-ik_2d_2}e^{-ikd}e^{ik_3d_3}e^{ik_4(d+d_3)}}{E}$$

where

$$T_3 = \frac{2N}{N+N_3},\quad T_4 = \frac{2N_3}{N_3+N_4}$$

or

$$T_3 = 1+r_3,\quad T_4 = 1-r_4$$

and

$$T_1 = 1-r_1,\quad T_2 = 1-r_2$$

Ultimate parameters of photon detectors

For simplified assessment of detection parameters of the photon detectors, the theory of ultimate normalized detectivity can be adopted, which is limited by thermal generation and recombination of carriers.

The current responsivity R_i of a photon detector is determined by the quantum efficiency η and the gain factor g. The quantum efficiency determines the number of electron-hole pairs generated per one falling photon. Whereas, the gain factor determines the number of carriers passing the contact per one generated electron-hole pair.

Spectral current responsitivity of a photon detector equals:

$$(16)\qquad R_i = \frac{\lambda}{hc}\cdot\eta\cdot q\cdot g$$

Electric current passing through detector's contacts is disturbed by noises because of statistic character of of the processes of thermal generation and recombination of the carriers.

It should be noticed that thermal fluctuation phenomena of generation and recombination of carriers can often be avoided by location of this process within the area of a semiconductor, where they have an insignificant influence because of small photoelectric gain. Processes G – R and the fluctuations connected with them cannot be avoided by any means.

The normalized detectivity D^* of a photon detector is the main parameter characterizing the normalized signal-to-noise ratio I_n of a detector.

$$D^* = \frac{R_i \cdot (A_0 \cdot \Delta f)^{1/2}}{I_n} \tag{17}$$

In connection with the above,

$$D^* = \frac{\lambda}{hc}\left(\frac{A_0}{A_e}\right)^{1/2} \cdot \left(\frac{\eta}{d^{1/2}}\right) \cdot \left[2(G+R)\right]^{-1/2} \tag{18}$$

The normalized detectivity D^* of the photon detectors is thus proportional to the wavelength λ, assuming that all material parameters are independent of wavelength and this is expressed by a simple fact that photon energy is inversely proportional to the wavelength. This dependency results that spectra detection increases in the linear manner together with wavelength, in the case of typical detectors within the range of short wavelengths.

For the assumed wavelength and operating temperature of a detector, detectivity can be optimized by increasing to the maximum: the ratio of the optical area to the electric field (A_o/A_e), the ratio of the quantum efficiency to the square root of the photosensitive element thickness $(\eta / d^{1/2})$ and by reducing the sum of the thermal generation and recombination of carriers velocities ($G + R$).

Thermal sensitivity and detectivity

For the qualitative assessment of the photon detectors operating within thermal imaging devices, the following parameters are proposed: the voltage thermal responsivity $R_{VT}(T_0)$ and the normalized the thermal detectvity $M^*(T_0)$, defined as:

$$R_{VT}(T_0) = \int_0^\infty R_v(\lambda) \frac{\partial W(\lambda, T)}{\partial T} d\lambda \tag{19}$$

$$M^*(T_0) = \int_0^\infty D^*(\lambda) \frac{\partial W(\lambda, T)}{\partial T} d\lambda \tag{20}$$

where:

$$W(\lambda, T) = c_1 \lambda^{-5} [\exp(\frac{C_2}{\lambda T}) - 1]^{-1} \tag{21}$$

These parameters connect the spectral characteristics of the voltage responsitivity R_v (λ) and normalized detectivity $D^*(\lambda)$ of detectors with spectral distribution of thermal radiation of the object under investigation $W(\lambda, T)$.

The voltage thermal responsivity allows the assessment of voltage magnitude generated on detector's contacts under the influence of individual temperature change of an object, whereas, thermal detectivity– noise-equivalent temperature difference (NETD) of a thermal imaging device. The above dependencies describe the actual state quite precisely. In practice, however, with the quality assessment of the photon detectors, the spectral characteristics are most often identified with the characteristics of an ideal photon counter fulfilling the following dependency:

$$R_v(\lambda) = \begin{cases} \frac{\lambda}{\lambda_{co}} R_v(\lambda_{co}) & dla \quad 0 \le \lambda \le \lambda_{co} \\ 0 & dla \quad \lambda > \lambda_{co} \end{cases} \tag{22}$$

hence,

$$R_{VT}(T_0) = R_v(\lambda_{co}) \int_0^\infty \frac{\lambda}{\lambda_{co}} \frac{\partial W(\lambda, T)}{\partial T} d\lambda \tag{23}$$

$$M^*(T_0) = D^*(\lambda_{co}) \int_0^\infty \frac{\lambda}{\lambda_{co}} \frac{\partial W(\lambda, T)}{\partial T} d\lambda$$

It can be seen from the abovementioned dependencies that the values of integrals depend only on the long-wavelength edge of photosensitivity (λ_{co}) and object temperature (T_0). They can be calculated by means of simple numerical integration.

Research results

Fig. 2 presents calculation results of the voltage responsitivity, whereas Fig.3 presents results of normalized detectivity of currently most popular high-temperature (T=300-200K) photon detectors - $Hg_{1-x}Zn_xTe$ photoresistors of monochromatic radiation (10.6μm) as a function of the content factor x.

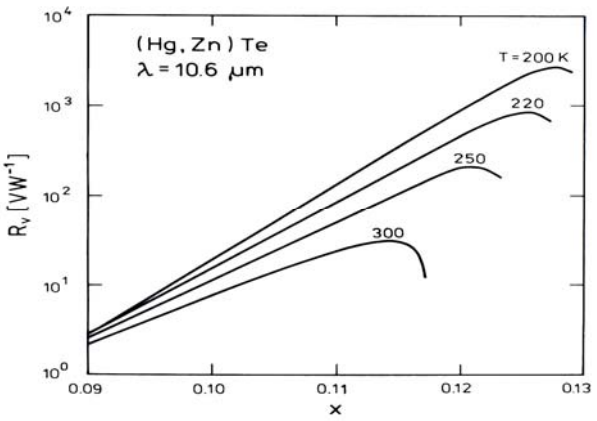

Fig. 2. Voltage responsivity of high-temperature (T=300-200K) $Hg_{1-x}Zn_xTe$ photoresistors of monochromatic radiation (10.6μm) as a function of the content factor x

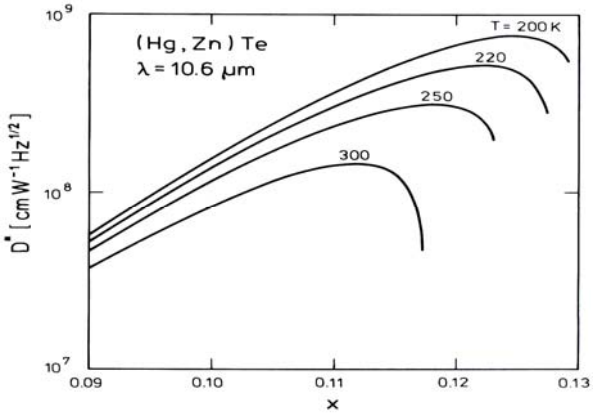

Fig. 3. Normalized detectivity of high-temperature (T=300-200K) $Hg_{1-x}Zn_xTe$ photoresistors for monochromatic radiation (10.6μm) as a function of the content factor x

Fig. 4 illustrates the resistance $R_{\square}$ of photosensitive elements optimally designed. The assessment of detection parameters has been conducted taking into consideration technological conditions, with the assumption that, optimal detection parameters of a photon detector are obtained for conduction band of a semiconductor, which is close to the energy of detected photons. This assumption is justified by acute dependency of absorption coefficient of a semiconductor on the wavelength at moderate doping.

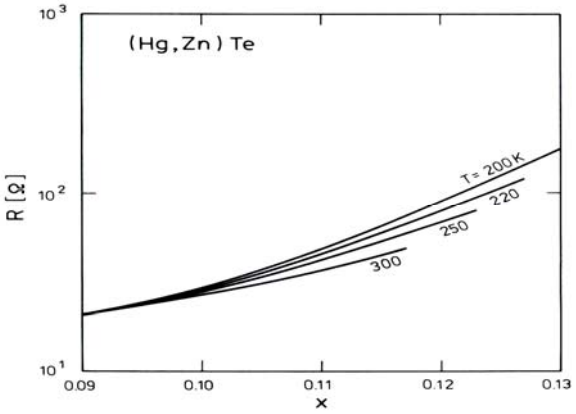

Fig. 4. Resistance $R_{\square}$ of high-temperature (T=300-200K) $Hg_{1-x}Zn_xTe$ photoresistors of monochromatic radiation (10.6μm) as a function of the content factor x

Fig. 5 presents calculation results of efficient radiation intensity for various models (4 models have been adopted) of detection structure and external quantum efficiency - Fig. 6 for the model ensuring the highest parameters for detection of monochromatic radiation.

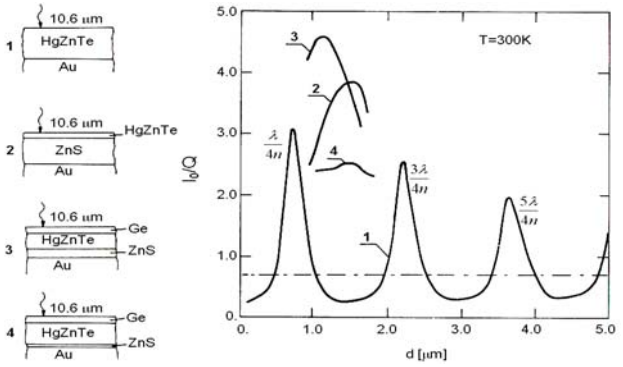

Fig. 5. Efficient radiation intensity penetrating a photosensitive element as a the function of its thickness for various models of detection structures

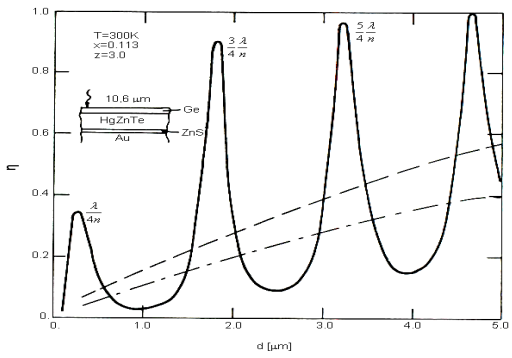

Fig. 6. External quantum efficiency for optimal detection structure as a function of photosensitive element thickness

Radiation intensity analysis (Fig. 5) within a photon element indicates that there exist discreet thicknesses of a photosensitive element for which the intensity on the illuminated surface obtains maximum values. For the first resonance thickness (at the assumption of a simple detection model – model 1) there is over threefold increase of intensity value. For the second resonance thicknesses, intensity on the illuminated surface rapidly decreases as a result of absorption of radiation within a photosensitive element. In practice it means that interference mechanism can be an efficient mechanism of increasing detection parameters of the photon detectors of monochromatic radiation only for the first resonance thicknesses of a photosensitive element. Optimization of the reflectance layer thickness (ZnS) and anti-reflectance (Ge) ensures over fourfold intensity increase (Fig.6) on the illuminated surface of a photosensitive element.

The number of generated carriers per absorbed photon depends on the efficiency of the radiation absorption within a photosensitive element. Efficient radiation absorption, in turn, may be significantly increased in thin photosensitive elements (Fig.5). The external quantum efficiency (Fig. 6) can be modulated by the interference effects. Oscillating character of radiation intensity within a photosensitive element is a driving force for an oscillating character of the external quantum efficiency. Application of the optical resonance cavity allows for multifold increase of external quantum efficiency for the three first resonance thicknesses of a photosensitive element.

The results of calculation indicate that there exist new and still not used possibilities in the construction of the photon detectors, and as a consequence in the construction of thermographic cameras of parameters which are higher in comparison with the commonly considered as their ultimate possibilities.

Ultimate normalized thermal detectivities of uncooled (T=300K) (Hg,Zn)Te photon detectors are presented in figures 7 - 9.

It is worth paying attention to the fact that with the increase of the object temperature (T_0), thermal detectivity increases (M*). Long-wavelength photosensitivity threshold ($\lambda_{co\ opt}$), ensuring achievement of the highest thermal detectvity, moves towards the shorter waves together with the increase of detected object, in accordance with a spectral radiation distribution ($W(\lambda, T)$). Detection of thermal radiation of objects at near room temperature (T=300K), with the use of (Hg,Zn)Te photon detectors is highly efficient within the medium infrared range.

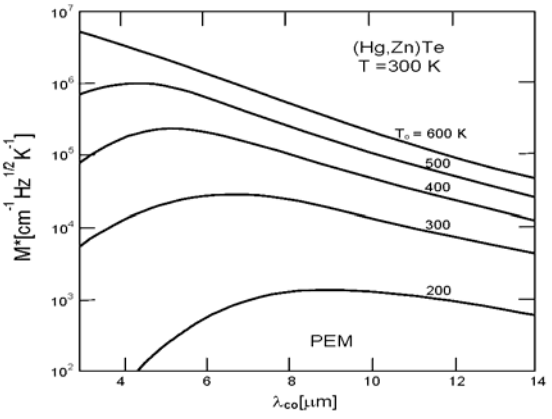

Fig. 7. Ultimate normalized thermal detectivity of uncooled (T=300K) (Hg,Zn)Te photoelectromagnetic detectors (PEM) as a function of the long-wavelength edge of photosensitivity (λ_{co}) and object temperature (T_0)

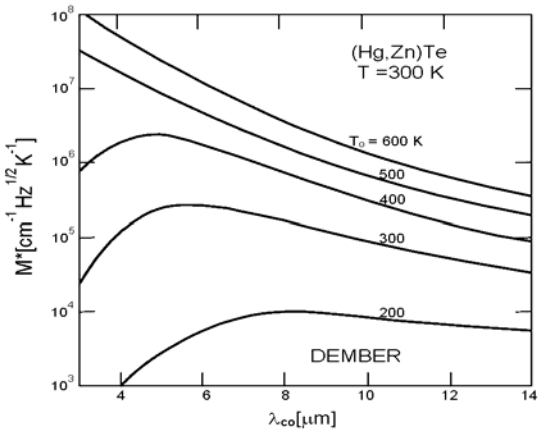

Fig. 8. Ultimate normalized thermal detectivity of uncooled (T=300K) (Hg,Zn)Te Dember detectors as a function the long-wavelength edge of photosensitivity (λ_{co}) and object temperature (T_0)

Plane characteristics of a thermal detectivity in this spectral range indicates that the choice of long-wavelength edge of photosensitivity is not critical for obtaining maximum thermal detectivity.

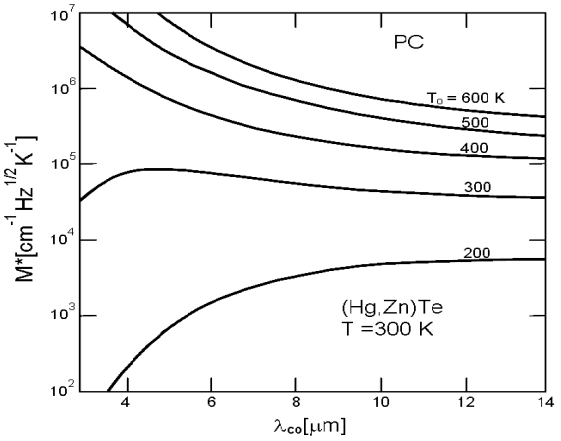

Fig. 9. Ultimate normalized thermal detectivity of uncooled (T=300K) (Hg,Zn)Te photoresistors (PC) as a function of the long-wavelength edge of photosensitivity (λ_{co}) and object temperature (T_0)

Summary

The problem of radiation detection has been defined for typical detection structure of a photon detector. The obtained results have been used for analysis of detection possibilities of new class of (Hg,Zn)Te photon detectors. New possibilities have been indicated for designing of the monochromatic radiation detectors. Real technological possibilities have been determined for achievement of normalized detectivity and voltage responsibilities of commonly used (Hg,Zn)Te photoresistors. Ultimate normalized thermal detections have been calculated for uncooled (T=300K), most popular photon detectors: the photoelectromagnetic detectors (PEM), the Dember detectors and the (Hg,Zn)Te photoresistors (PC) sa a function of the long-wavelength edge of photosensitivity (λ_{co}) and object temperature (T_0).

REFERENCES

[1] Cyran K. A., Niedziela T.: Optimization method of feature extractor for automatic pattern recognition system of motor vehicles, Archives of Transport, **XXI**, 1-2, 2009, 5-25

[2] Cyran K. A., Niedziela T.: Opto-electronic method of pattern recognition of motor vehicles in spatial frequency domain, Archives of Transport, **XXI**, 1-2, 2009, 27-47

[3] Cyran K. A., Niedziela T.: Automatic recognition of the type of road vehicles with the use of optimised ring-wedge detector and neural network, Archives of Transport , **XVIII**, 3, 2006, 23-36

[4] Cyran K. A., Niedziela T.: Infrared images in automatic recognition of the type of road obstacle in a fog, Archives of Transport, **XVIII**, 4, 2006, 29-38

[5] Niedziela T., Krukar W.: Method of automatic recognition of registration plates of motor vehicles. Oficyna Wydawnicza Politechniki Warszawskiej, Transport Scientific Papers, 57, 2006, 67-86

[6] Niedziela T.: Near-room temperature narrow-bandgap infrared photon detectors. Research Works of Air Force Institute of Technology, Warsaw, 1, 1996, 1-300

[7] Piotrowski J., Niedziela T.: Mercury zinc telluride long-wavelength high temperature photoconductors, Infrared Physics, **30**, 2, 1990, 113-119

[8] Niedziela T., Piotrowski J., Application of mercury zinc telluride for high temperature photoconductors, Journal of Technical Physics, **31**, 3-4, 1990, 295-304

[9] Kamiński B., Niedziela T.: Distribution of electric field and intensity of radiation in a photosensitive layer located in optical resonance cavity, Journal of Technical Physics, **31**, 3-4, 1990, 305-318

[10] Niedziela T.: Influence of optical resonance cavity on operation of far infrared (Hg,Zn)Te photoresistors, Electron Technology , **24**, 1/2, 1990, 71-85

[11] Niedziela T.: (Hg,Zn)Te photon detectors for 10.6um laser radiation with optical resonanse cavity, Second International Meeting INFRARED TECHNOLOGY AND APPLICATION, London, 1990, 25-29

[12] Niedziela T: Carrier lifetime in $Hg_{1-x}Zn_xTe$ at 300K, Journal of Technical Physics, **30**, 3-4, 1989, 319-326

[13] Niedziela T, Rogalski A., Piotrowski J.: Calculation of the carrier lifetime in $Hg_{1-x}Zn_xTe$, Infrared Physics 5, 1988, 311-319

[14] Born W., Wolf E.: Principles of optics, Pergamon Press, 1968.

***Autor**: prof dr hab. inż. Tadeusz Niedziela, Politechnika Warszawska, Wydział Transportu, ul. Koszykowa 75, 00-680 Warszawa, E-mail:tadeuszniedziela@poczta.onet.pl*